Taylor & Francis
Taylor & Francis Group

Applied Earth Science

Transactions of the Institutions of Mining and Metallurgy: Section B

ISSN: 0371-7453 (Print) 1743-2758 (Online) Journal homepage: http://www.tandfonline.com/loi/yaes20

A black shale protolith for gold-tellurium mineralisation in the Dalradian Supergroup (Neoproterozoic) of Britain and Ireland

J. Parnell, M. Perez, J. Armstrong, L. Bullock, J. Feldmann & A. J. Boyce

To cite this article: J. Parnell, M. Perez, J. Armstrong, L. Bullock, J. Feldmann & A. J. Boyce (2017) A black shale protolith for gold-tellurium mineralisation in the Dalradian Supergroup (Neoproterozoic) of Britain and Ireland, Applied Earth Science, 126:4, 161-175, DOI: 10.1080/03717453.2017.1404682

To link to this article: https://doi.org/10.1080/03717453.2017.1404682

Published online: 30 Nov 2017.

APPLIED EARTH SCIENCE (TRANS. INST. MIN. METALL. B), 2017
VOL. 126, NO. 4, 161–175
https://doi.org/10.1080/03717453.2017.1404682

The Institute of Materials, Minerals and Mining
AusIMM THE MINERALS INSTITUTE
Taylor & Francis
Taylor & Francis Group

A black shale protolith for gold-tellurium mineralisation in the Dalradian Supergroup (Neoproterozoic) of Britain and Ireland

J. Parnell [a], M. Perez[b], J. Armstrong[a], L. Bullock[a], J. Feldmann[b] and A. J. Boyce[c]

[a]School of Geosciences, University of Aberdeen, Aberdeen, UK; [b]Trace Element Speciation Laboratory (TESLA), Department of Chemistry, University of Aberdeen, Aberdeen, UK; [c]Scottish Universities Environmental Research Centre, East Kilbride, Glasgow, UK

ABSTRACT

The Dalradian Supergroup of Britain and Ireland is mineralised by gold-tellurium vein deposits. The host succession includes carbonaceous, pyritic shales (pelites) which were a source of trace elements, including gold and tellurium. LA-ICP-MS mapping of pyrite crystals shows that late stages are enriched in gold, tellurium and lead, representing concentration of these elements during metamorphism and related hydrothermal activity. The sulphur isotope composition of the pyrite varies with stratigraphic position, reflecting an origin for the pyrite in the depositional environment through microbial sulphate reduction. Where pyrite was converted to pyrrhotite, trace element contents are much lower, indicating element liberation during metamorphism. These observations are consistent with a model of black shale protoliths for orogenic gold deposits.

ARTICLE HISTORY
Received 26 July 2017
Revised 7 November 2017
Accepted 7 November 2017

KEYWORDS
Gold; tellurium; selenium; Dalradian; Neoproterozoic; pyrite; pyrrhotite; Scotland; Ireland; microbial sulphate reduction

Introduction

The Neoproterozoic Dalradian Supergroup in Scotland and Ireland (Figures 1 and 2) is mineralised by gold (Au) at numerous localities, some of which are being commercially exploited at the time of publication (Figure 2). Vein-hosted Au mineralisation, cross-cutting Dalradian metasediments, is dated variably to Ordovician to early Devonian (Treagus et al. 1999; Rice et al. 2016). Previous models for the Au mineralisation suggest that it may be attributed at least in part to magmatic fluids (Curtis et al. 1993; Parnell et al. 2000; Tanner 2012; Hill et al. 2014; Jenkin et al. 2017), or, alternatively, to meteoric fluids (Craw and Chamberlain 1996) or metamorphism (Pitcairn et al. 2015). This ambiguity over the role of magmatic fluids is reflected in broader models for orogenic gold deposits (Goldfarb and Groves 2015; Wyman et al. 2016). Where the Au in the Dalradian Supergroup has been identified in telluride mineralisation, in Ireland (Parnell et al. 2000) and Scotland (Pattrick et al. 1988; Earls et al. 1992), the mineralising fluids for the tellurium (Te)-bearing stage have been interpreted as magmatic. The Dalradian Supergroup also includes exhalative barite and base metal sulphide deposits (Willan and Coleman 1983; Hall 1993; Moles et al. 2014), especially in the Easdale Subgroup of the Argyll Group, and younger (post-Au) hydrothermal lead (Pb) deposits (Pattrick and Russell 1989). The Easdale Subgroup includes pyritic black carbonaceous shales over an outcrop length of at least 450 km outcrop length in Ireland and the Scottish mainland. This is significant, as one model for Au mineralisation in orogenic belts is based on the uptake of trace elements onto organic matter from seafloor exhalative fluids, followed by incorporation into early pyrite and concentration during metamorphism (Large et al. 2009). The black shales of the Easdale Subgroup meet the model criteria of high content of organic matter, evidence of exhalative activity, widespread pyrite precipitation, and overprinting by regional metamorphism. Therefore, the black shales deserve assessment as a source for Au mineralisation.

The concentrations of trace elements in pyrite can be assessed using laser ablation-inductively coupled plasma-mass spectrometry (LA-ICP-MS), which allows detection of low levels of trace element enrichment, maps spatial variations, and thereby discriminates different generations of pyrite precipitation (Wagner et al. 2007; Large et al. 2007; Diehl et al. 2012). This study uses LA-ICP-MS measurements of pyrite, supported by whole rock compositions, in the Dalradian Supergroup of Scotland and Ireland to assess the availability of trace elements in black shales and the possibility of a black shale protolith for Dalradian-hosted Au-Te mineralisation. In particular, we address:

(i) Whether early (syn-diagenetic) and late (metamorphic-hydrothermal) generations of pyrite can be distinguished, allowing assessment of trace element evolution.
(ii) Where early pyrite can be identified, whether there is evidence for trace element enrichment at an early stage.

CONTACT J. Parnell j.parnell@abdn.ac.uk School of Geosciences, University of Aberdeen, Aberdeen AB24 3UE, UK

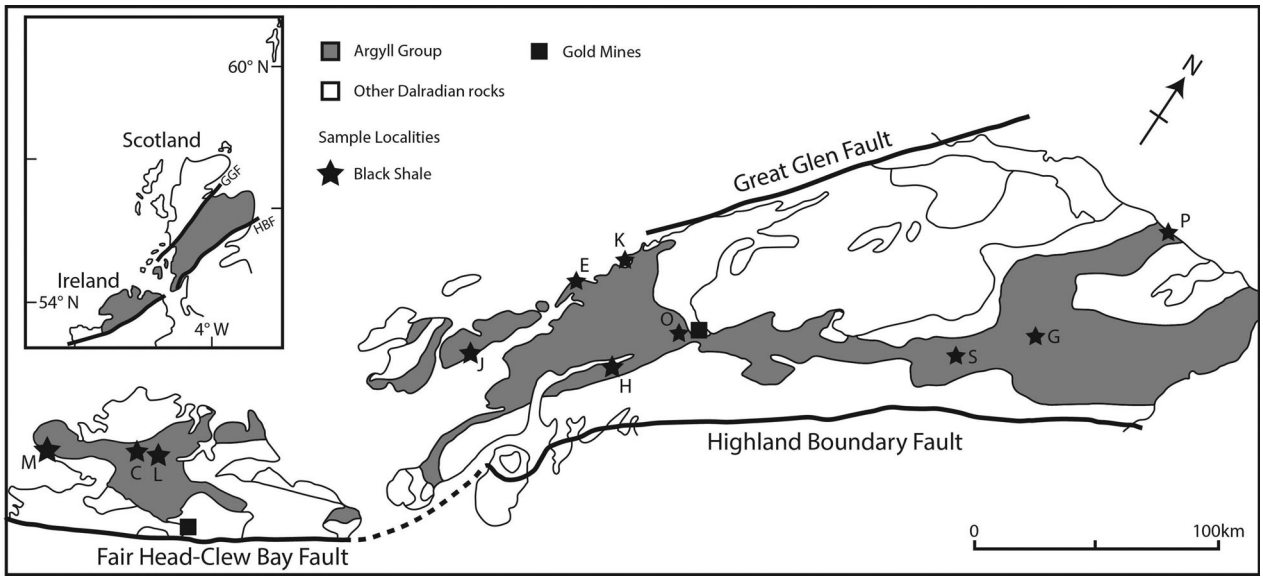

Figure 1. Sample map (after Prave et al. 2009). C: Cullion; E: Easdale; G: Glenbuchat; H: Strachur; J: Jura Forest; K: Kerrera; L: Bellanamore; M: Muckross; O: Strath Orchy; P: Portsoy; S: Glen Shee.

(iii) Where late pyrite can be identified, whether there is evidence for mobility and/or concentration of trace elements, especially Au, during metamorphism and related hydrothermal fluid flow.
(iv) Whether trace element enrichments are preserved or lost during conversion from pyrite to pyrrhotite during metamorphism.

Geological setting

The Dalradian Supergroup is bounded by the Highland Boundary Fault and Great Glen Fault (Figure 2). The succession (Figure 1) was deposited on the eastern margin of Laurentia, from the mid-Neoproterozoic to Cambrian, and includes marine siliciclastic and carbonate sediments, and limited glaciogene and volcanic rocks (Anderton 1985; Stephenson et al. 2013). Towards the top of the >10 km succession, the Argyll Group includes carbonaceous pelites (black shales) and diamictites, and also hosts stratabound exhalative barite and base metal sulphide mineralisation (Moles et al. 2014). Dating of the succession is sparse (Figure 2), but the most prominent diamictite unit, the Port Askaig Formation, is correlated to the global Sturtian tillite (Prave et al. 2009), and volcanics at the top of the Argyll Group are dated at about 600 Ma (Dempster et al. 2002). The Dalradian rocks were deformed and regionally metamorphosed, during and following Ordovician closure of the Iapetus Ocean. Metamorphism varies from greenschist facies to amphibolite facies (Harte 1988).

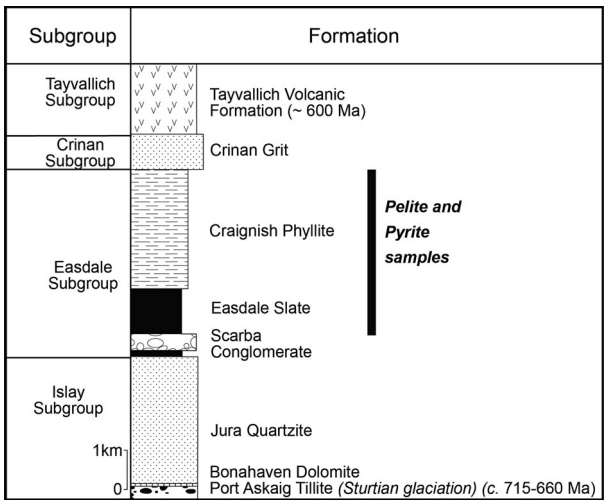

Figure 2. Stratigraphic succession for Dalradian Argyll Group, south west Scotland, showing age constraints. Pyrite sampled from Easdale Slate and Craignish Phyllite in Easdale Subgroup.

Methodology

Sampling

Sulphide-bearing samples were collected from carbonaceous shales in the Easdale Subgroup (Easdale Slate and Craignish Phyllite/Termon Pelite). Samples at 11 localities (Figure 2, Table 1) spanned a strike length of 450 km over the Dalradian outcrop of Scotland and Ireland. The sulphides are pyrite, excepting at Strachur and Portsoy, where the dominant sulphide is pyrrhotite. Most of the samples are from regions metamorphosed to greenschist facies (as mapped by Fettes 1979), but some including the two pyrrhotite-bearing localities are in amphibolite facies (Table 1).

Whole rock

Trace element content (Table 1, Figures 3 and 4) was measured in shale samples using inductively coupled plasma-mass spectrometry (ICP-MS) at the ALS Minerals Loughrea Laboratory, Ireland. Samples of ~30 g rock were milled and homogenised, and 0.25 g digested with perchloric, nitric, hydrofluoric and hydrochloric

Table 1. Whole rock compositions for Dalradian Argyll Subgroup carbonaceous shales.

Units		Locality	Grid Ref.	Grade	Ag ppm	Bi ppm	Co ppm	Cu ppm	Mo ppm	Ni ppm	Pb ppm	Re ppm	Se ppm	Te ppm	Zn ppm	S %	TOC %
Sample ID	Lithology																
STORM 72	Easdale Slate	Cullion	C 002018	Greenschist	0.13	0.34	13.6	35.4	0.40	27.0	18.0	0.001	2.3	0.06	59	2.46	0.80
STORM 217	Easdale Slate	Cullion	C 002018	Greenschist	0.07	0.03	19.6	8.6	0.25	9.2	6.0	0.001	0.5	0.02	17	0.29	1.57
STORM 218	Easdale Slate	Cullion	C 002018	Greenschist	0.06	0.03	18.8	10.5	0.19	8.7	6.5	0.001	0.5	0.01	14	0.27	1.52
STORM 219	Easdale Slate	Cullion	C 002018	Greenschist	0.10	0.40	41.8	37.5	0.61	37.2	12.1	0.001	1.1	0.04	160	1.07	1.05
STORM 220	Easdale Slate	Easdale	NM 746173	Greenschist	0.05	0.11	7.7	20.8	0.57	15.9	7.3	0.001	0.4	0.02	112	0.76	0.24
STORM 221	Easdale Slate	Easdale	NM 746173	Greenschist	0.09	0.20	22.0	50.1	0.39	55.6	16.8	0.001	0.5	0.03	101	0.65	0.40
STORM 243	Easdale Slate	Easdale	NM 746173	Greenschist	0.07	0.10	15.2	28.3	0.30	27.7	11.2	0.001	0.7	0.02	83	1.37	0.34
STORM 244	Easdale Slate	Easdale	NM 746173	Greenschist	0.17	0.40	25.2	65.6	0.52	53.5	27.5	0.001	1.0	0.08	103	1.55	0.22
TEREAS 7	Easdale Slate	Easdale	NM 746173	Greenschist	0.07	0.18	19.0	29.2	0.31	35.1	16.1	0.003	1.0	0.05	118	1.06	0.91
TEREAS 8	Easdale Slate	Easdale	NM 746173	Greenschist	0.08	0.24	23.0	36.7	0.20	44.3	20.8	0.002	1.0	0.05	116	1.00	0.46
TEREAS 10	Easdale Slate	Easdale	NM 746173	Greenschist	0.13	0.27	23.1	20.1	0.25	22.7	22.4	0.004	2.0	0.06	40	3.80	0.51
STORM 71	Easdale Slate	Glenshee	NO 137782	Amphibolite	0.95	1.04	55.4	88.5	13.55	79.3	544.0	0.004	5.1	0.12	225	3.05	1.94
STORM 228	Easdale Slate	Glenshee	NO 137782	Amphibolite	0.86	1.06	48.6	86.1	12.60	69.1	555.0	0.004	4.6	0.12	214	2.16	1.33
STORM 241	Easdale Slate	Jura Forest	NR 535701	Greenschist	0.03	0.09	9.3	24.5	1.98	2.7	3.1	0.002	0.6	0.01	58	0.31	1.09
STORM 242	Easdale Slate	Jura Forest	NR 535701	Greenschist	0.13	0.42	24.8	120.5	0.77	28.4	32.7	0.001	0.8	0.09	79	0.64	0.37
STORM282	Easdale Slate	Muckross	G 615745	Amphibolite	0.13	0.33	51.4	34.2	0.66	28.4	16.1	0.002	0.8	0.02	81	1.29	
STORM 69	Easdale Slate	Portsoy	NJ 586664	Amphibolite	0.12	0.20	49.4	40.8	0.87	32.4	16.5	0.001	2.4	0.02	26	1.62	4.14
STORM 225	Easdale Slate	Portsoy	NJ 586664	Amphibolite	0.05	0.24	29.1	57.2	2.17	52.2	14.8	0.003	3.7	0.05	41	2.28	2.86
STORM 226	Easdale Slate	Portsoy	NJ 586664	Amphibolite	0.05	0.29	36.0	47.9	2.46	59.3	13.3	0.002	1.7	0.04	54	1.48	3.43
STORM 227	Easdale Slate	Portsoy	NJ 586664	Amphibolite	0.11	0.26	23.7	42.6	1.13	28.3	12.4	0.002	3.8	0.03	28	1.19	3.22
STORM 73	Easdale Slate	Strathorchy	NN 194274	Greenschist	0.50	0.16	76.3	185.5	0.42	145.0	16.7	0.001	5.2	0.13	49	8.53	0.97
STORM 148	Easdale Slate	Strathorchy	NN 194274	Greenschist	0.17	0.15	46.6	80.7	1.11	51.2	11.7	0.002	3.1	0.04	17	2.52	1.29
STORM 222	Easdale Slate	Strathorchy	NN 194274	Greenschist	0.07	0.18	14.6	38.3	1.71	34.5	12.9	0.001	2.7	0.04	134	1.46	2.79
STORM 223	Easdale Slate	Strathorchy	NN 194274	Greenschist	0.22	0.04	34.7	94.1	0.92	135.5	21.4	0.001	4.7	0.03	82	3.65	0.83
STORM 253	Easdale Slate	Strathorchy	NN 194274	Greenschist	0.12	0.16	25.4	45.6	0.66	48.7	14.7	0.003	2.8	0.04	122	1.94	0.77
STORM 224	Termon Pelite	Bellanamore	B 966022	Greenschist	0.54	1.79	32.7	85.8	6.12	7.4	172.0	0.004	2.1	0.25	34	2.04	0.14
STORM 245	Termon Pelite	Bellanamore	B 966022	Greenschist	0.27	0.60	26.4	73.1	6.19	23.6	65.8	0.003	2.0	0.09	45	2.76	0.12
STORM 246	Termon Pelite	Bellanamore	B 966022	Greenschist	0.04	0.11	24.4	28.0	3.65	26.0	8.4	0.002	0.9	0.03	126	0.98	0.27
STORM 247	Termon Pelite	Bellanamore	B 966022	Greenschist	0.05	0.10	17.8	15.7	3.97	18.6	18.2	0.003	0.9	0.01	110	0.58	0.33
TERCAT 7	Termon Pelite	Bellanamore	B 966022	Greenschist	1.08	2.56	42.1	107.5	4.88	7.6	173.5	0.007	4.0	0.25	59	3.04	0.18
TERCAT 9	Termon Pelite	Bellanamore	B 966022	Greenschist	0.95	2.00	60.4	175.0	6.62	12.5	180.5	0.004	5.0	0.20	56	4.63	0.17
TERCAT 10	Termon Pelite	Bellanamore	B 966022	Greenschist	0.52	1.45	57.9	225.0	1.16	7.9	148.0	0.004	2.0	0.27	37	4.05	0.11
STORM 70	Craignish Phyllite	Loch Melfort	NM 838130	Greenschist	0.06	0.17	24.6	19.2	2.45	28.5	18.0	0.005	1.8	0.03	80	0.94	0.09
STORM 229	Craignish Phyllite	Loch Melfort	NM 838130	Greenschist	0.08	0.21	23.1	20.6	1.74	30.1	33.7	0.002	1.8	0.02	106	0.91	0.03
STORM 312	Craignish Phyllite	Strachur	NN 087024	Amphibolite	0.02	0.15	30.5	39.7	0.08	34.2	1.6	0.002	1	0.03	93	0.39	
Mean values					0.23	0.46	31.26	60.54	2.34	37.95	64.85	*	2.13	0.07	82.26	1.91	1.05
Average shale/pelite values (Hu and Gao, 2008) – $n = 21$; Se = Stüeken et al. (2015); Ag = Turekian and Wedepohl (1961)					0.07	0.46	15.77	35.3	1.04	38.9	23.3	0.001	1.3	0.05	83		

*Published values for Re in shale vary widely.

acids to near dryness. The residue was topped up with dilute hydrochloric acid, and analysed using a Varian 725 instrument. Samples with high concentrations were diluted with hydrochloric acid to make a solution of 12.5 mL, homogenised, then analysed by ICP-MS. Results were corrected for spectral inter-element interferences. The limits of detection/resolution are 0.05 and 10,000 ppm. Geological Certified Reference Materials (CRMs) utilised included MRGeo08 (mid-range multi-element CRM), GBM908-10 (base metal CRM), OGGeo08 (ore grade multi-element CRM) and GEOMS-03 (multi-element CRM). Results for CRM analysis were within the anticipated target range (upper and lower bound) for each metal and standard. Duplicate analysis of one sample produced reported values within the acceptable range for laboratory duplicates, with an average relative percent difference of 4%.

LA-ICP-MS

Trace element analysis was performed using a New Wave laser ablation system UP213 nm (New Wave Research, Fremont, CA) coupled to a inductive coupled plasma-mass spectrometer (ICP-MS) Agilent 7900 (Agilent Technologies, Tokyo, Japan) at the University of Aberdeen Trace Element Speciation Laboratory. The laser beam had a round spot size of 100 μm moving in a straight line, 10 Hz repetition rate and 50 μm s^{-1} ablation speed with 1 J cm^2 energy. Before ablation, a warm-up of 15 s was applied with 15 s delay between each ablation. The following isotopes were monitored (dwell time): ^{57}Fe (0.001 s), ^{65}Cu (0.001 s) ^{75}As (0.05 s), ^{78}Se (0.1 s), ^{82}Se (0.1 s), ^{107}Ag (0.1 s), ^{125}Te (0.1 s), ^{126}Te (0.1 s), ^{197}Au (0.1 s), ^{202}Hg (0.1 s), ^{208}Pb (0.05 s) and ^{209}Bi (0.1 s). Settings parameters were optimised daily by using a NIST Glass 612 (NIST Gaithersburg MD), to obtain the maximum sensitivity and to ensure low oxide formation. Oxide formation was assessed by monitoring the ratio $^{232}Th^{16}O^{+}/^{232}Th^{+}$ (as 248/232) and maintained under 0.3%. In order to remove possible interferences which could affect selenium measurement, a reaction cell was used with hydrogen gas. The MASS-1 Synthetic Polymetal Sulphide standard (USGS, Reston, VA) was used to provide semi-quantification by calculating the ratio of concentration, (μg g^{-1})/counts per seconds, and multiplying this ratio by the sample counts. For this, three lines were ablated with at least 50 measures per lines and the average was used for calculations. The relative standard deviation was below 10% for each element measured. The gold concentration in the reference material is not certified and was described by Wilson et al. (2002) as strongly heterogeneous, so was used for semi-quantification but with a high standard deviation.

Element maps (Figures 5–9) were prepared for iron, arsenic (the most abundant trace element in diagenetic pyrite), gold and tellurium (potential protoliths for

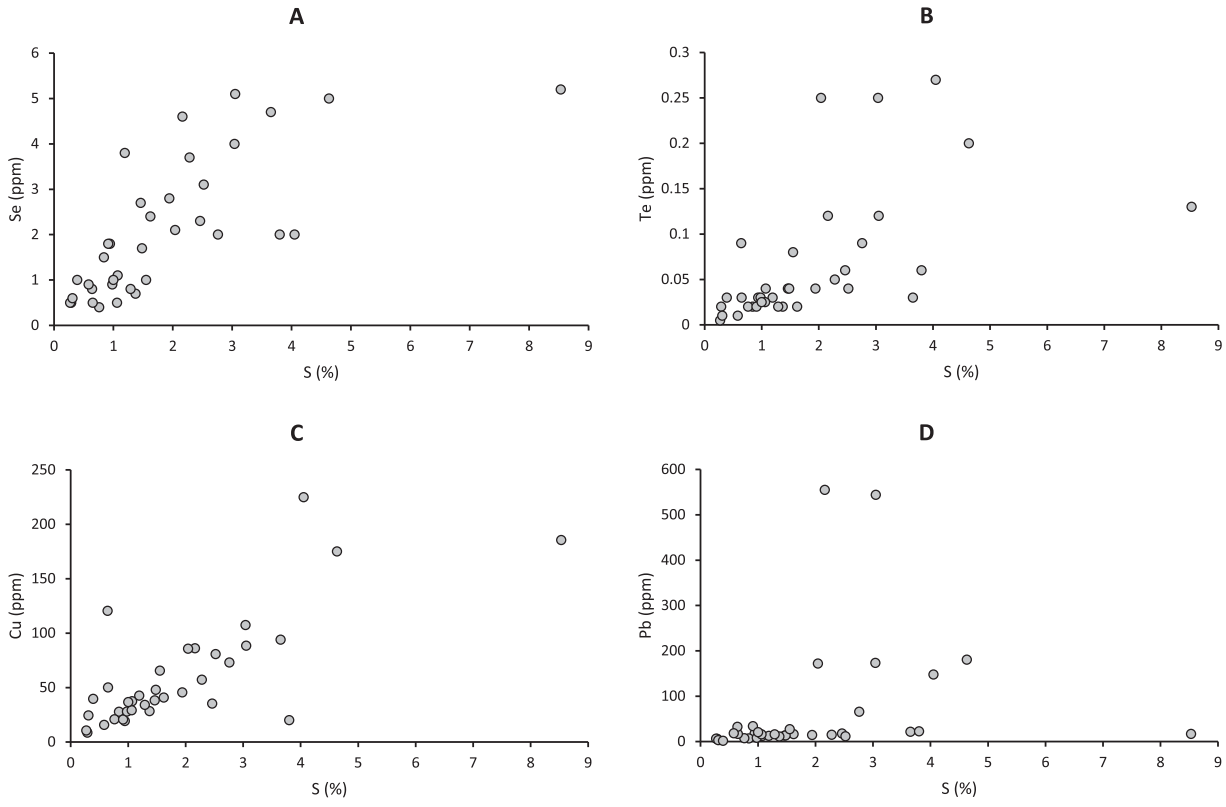

Figure 3. Cross-plots of whole rock sulphur content against whole rock contents of (A) selenium, (B) tellurium, (C) copper, and (D) lead. Selenium, tellurium and copper show broad patterns of increasing content with sulphur. Lead shows a bimodal distribution, reflecting presence or absence of lead-rich rims on pyrite.

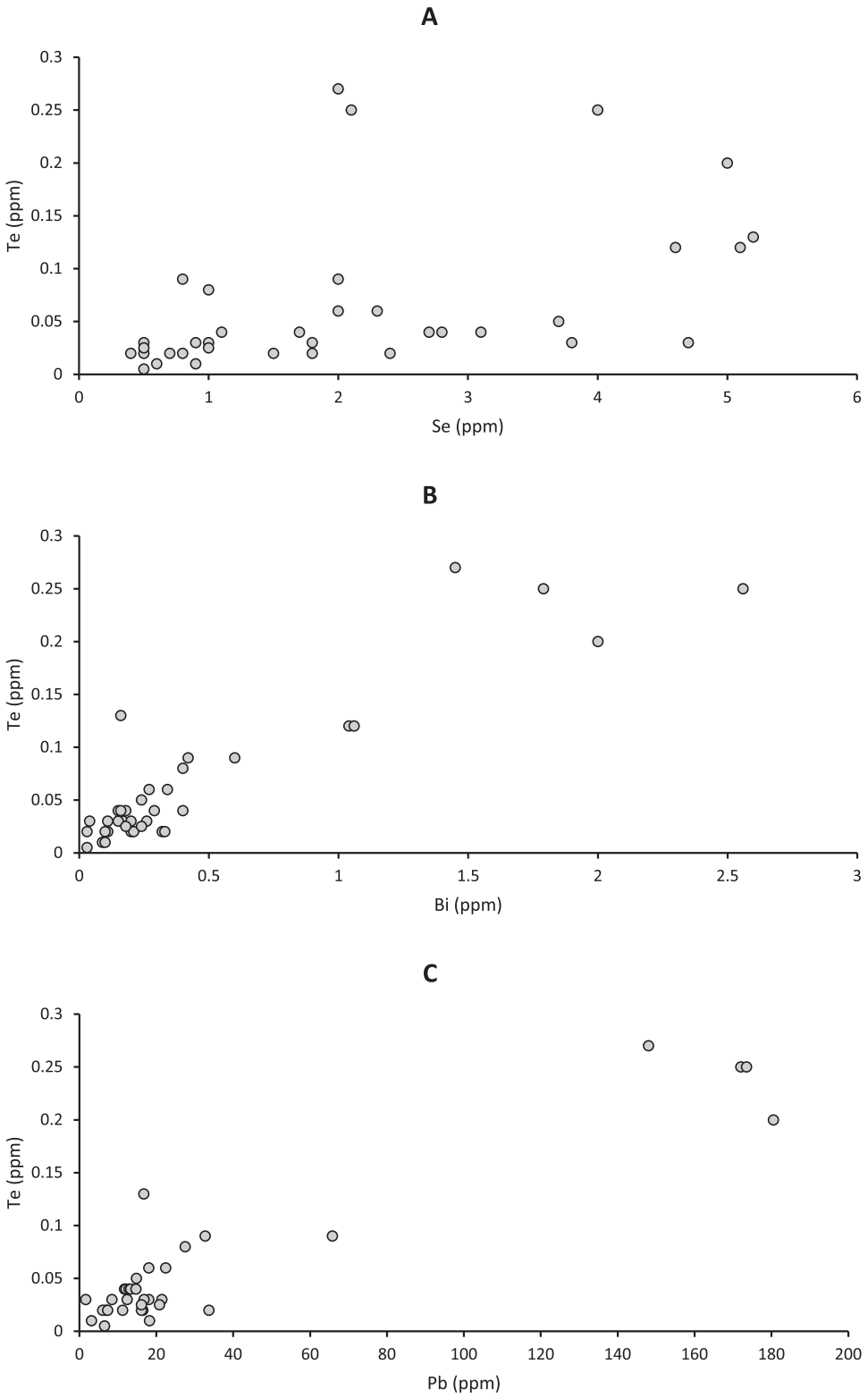

Figure 4. Cross-plots of whole rock tellurium content against whole rock contents of (A) selenium, (B) bismuth, and (C) lead. Tellurium broadly increases with Bi and Pb. Plot (C) omits two high Pb values between 500 and 600 ppm, shown in Figure 3(D).

gold telluride mineralisation), lead (as the Dalradian hosts hydrothermal Pb mineralisation), and selenium (commonly concentrated with Te, but liable to fractionate with Pb rather than Au mineralisation). Quantification was made for Se and Te (Figure 10), and semi-quantification was made for Au for a set of pyrite samples from Bellanamore, Ireland (Figure 11). Measurements of Te and Au are compared with data for Phanerozoic (Ordovician and Carboniferous) black shales from Britain and Ireland.

S isotopes

Samples of pyrite from the Easdale Slate at Easdale, and the Craignish Phyllite at Loch Melfort and Bellanamore were prepared for conventional sulphur isotopic analysis

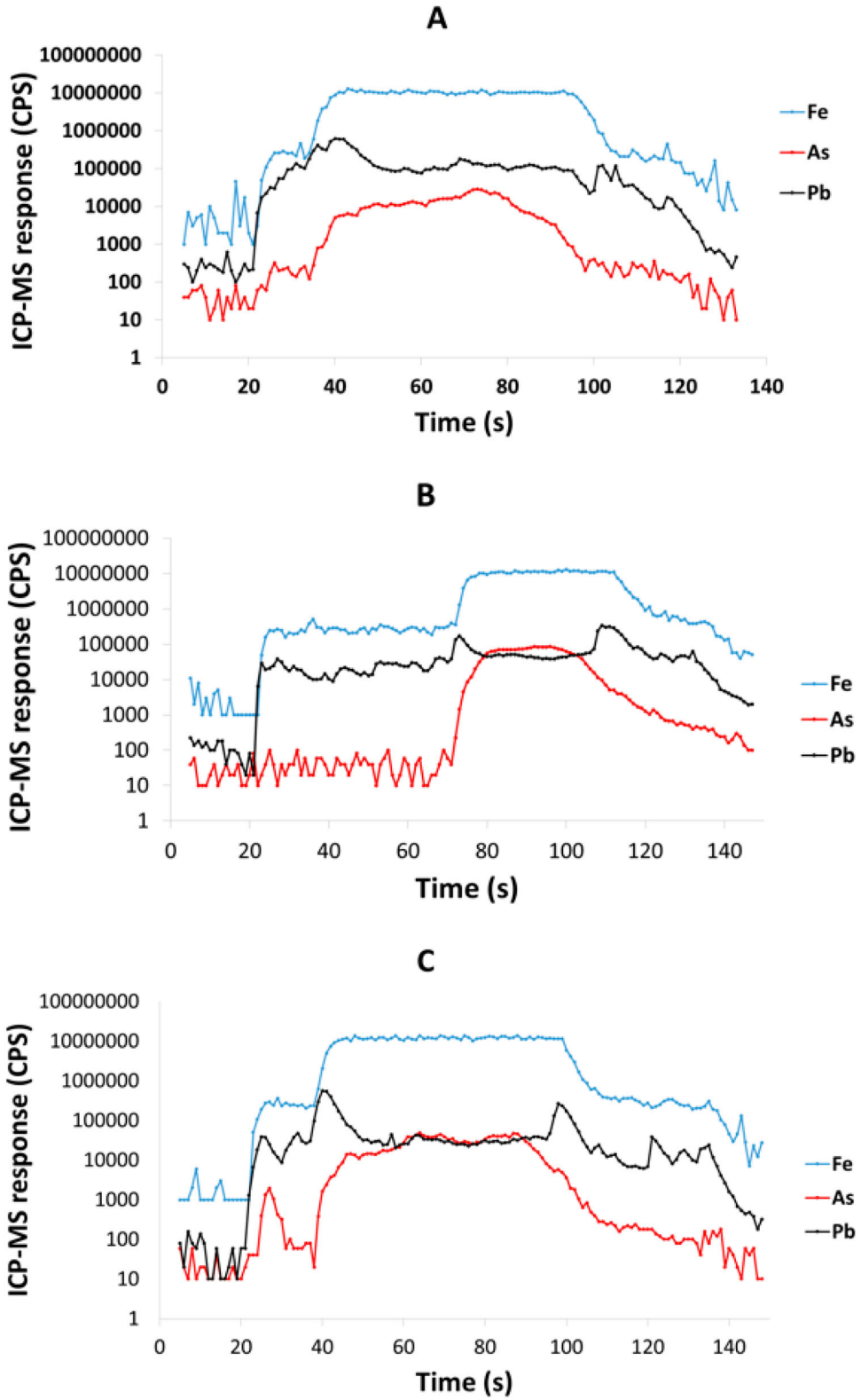

Figure 5. LA-ICP-MS profiles for Fe, As and Pb through pyrite crystals in Easdale Subgroup from (A) Jura Forest, (B) Easdale, and (C) Bellanamore. In all three samples, As exhibits a higher content in the core of the crystal, while Pb exhibits enrichment in the rim.

at the Scottish Universities Environmental Research Centre (SUERC) by standard techniques (Robinson and Kusakabe, 1975). Five to 10 mg was utilised for isotopic analysis. SO_2 gas was liberated by combusting the sulphides with excess Cu_2O at 1075°C, *in vacuo*. Liberated gases were analysed on a VG Isotech SIRA II mass spectrometer, and standard corrections applied to raw $\delta^{66}SO_2$ values to produce true $\delta^{34}S$. All SO_2 gases were analysed on a VG Isotech SIRA II mass spectrometer. The standards employed were the international standard NBS-123 and IAEA-S-3, and SUERC standard CP-1. These gave $\delta^{34}S$ values of +17.1‰, −31.6‰ and −4.6‰, respectively, with 1σ reproducibility better than ±0.2‰ around the time of these analyses. Data are reported in $\delta^{34}S$ notation as per mil (‰) variations from the Vienna Canyon Diablo Troilite (V-CDT) standard.

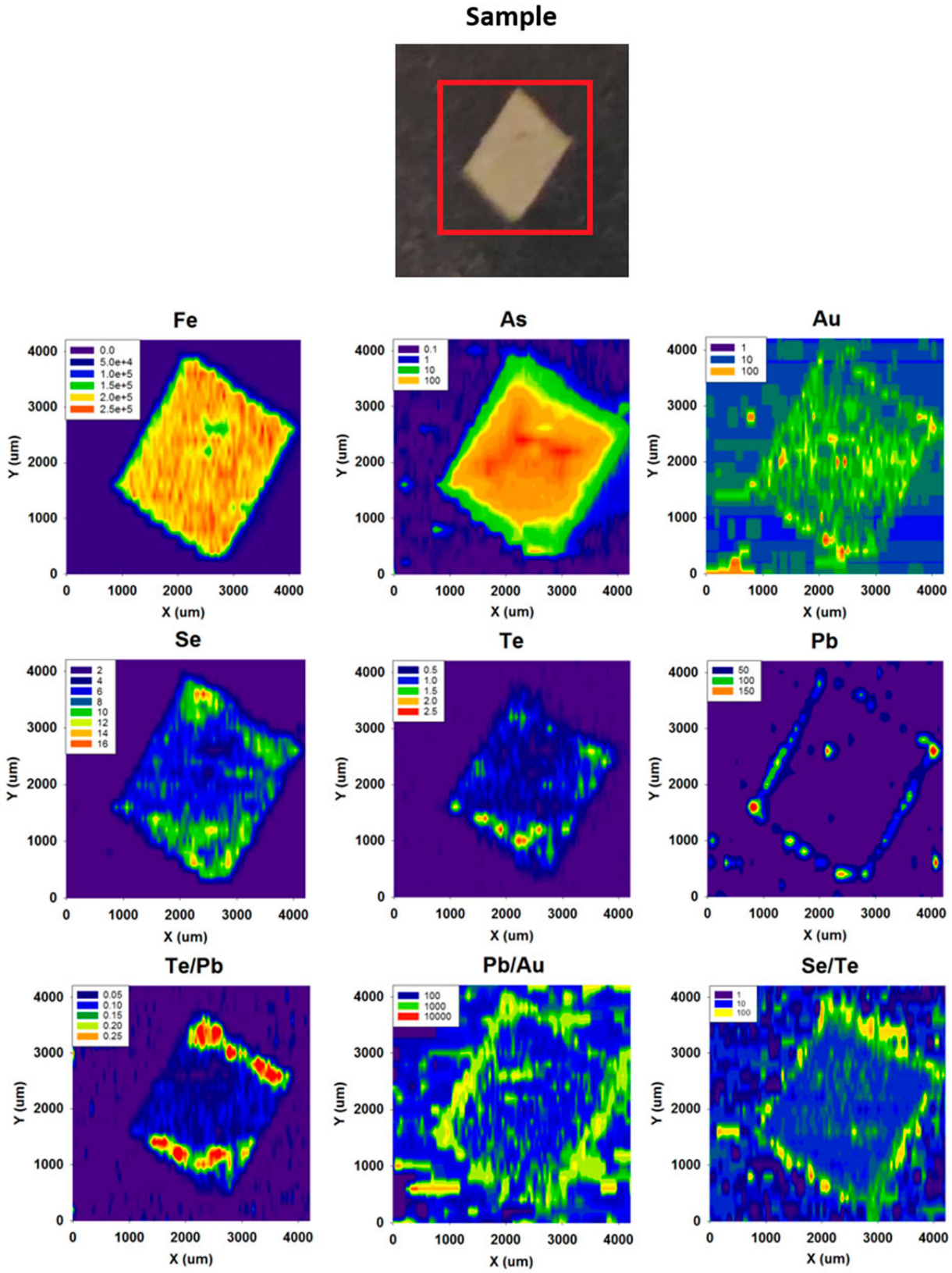

Figure 6. LA-ICP-MS element and element ratio maps for pyrite crystal, Termon Pelite, Bellanamore, Ireland. Note Au, Te and Se through core; Element ratio maps show Pb and Se enriched in outer rim, and Te-rich enrichment in inner rim.

SEM

Sulphide samples were examined using an ISIS ABT-55 scanning electron microscope with Link Analytical 10/55S EDAX facility, to identify any mineral inclusions that would appear as point sources in LA-ICP-MS maps, and distinguish pyrite from pyrrhotite (Figure 12).

Results

Whole rock

Previous measurements showed that sulphur levels and Total Organic Carbon contents in the shales of the Easdale Subgroup are high (Bata and Parnell 2014). Both

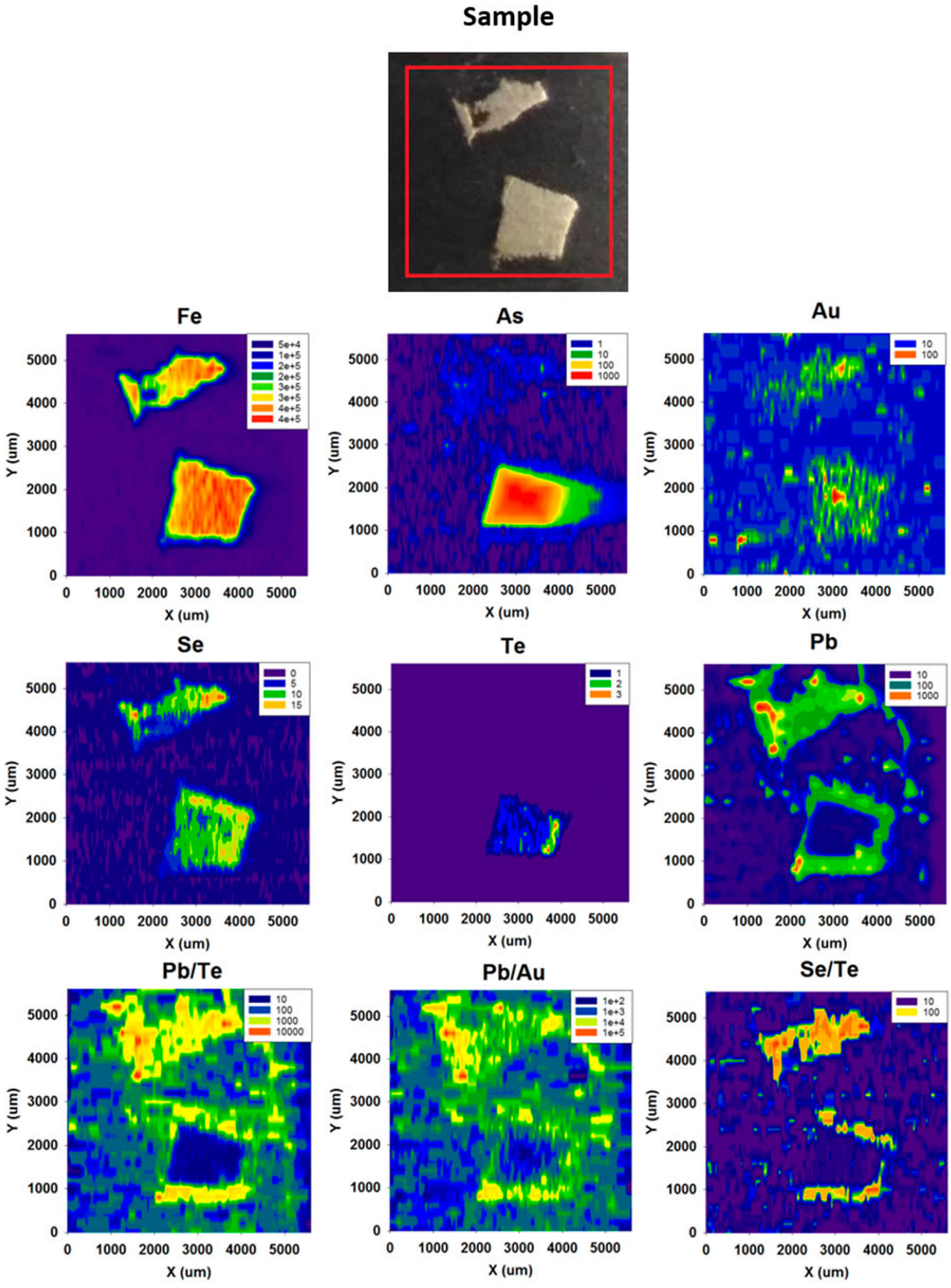

Figure 7. LA-ICP-MS element and element ratio maps for two adjacent pyrite crystals, Easdale Slate, Easdale, Scotland. One crystal is cut through both core and rim, while other is cut through rim only, giving distinct patterns. Note core is rich in As, Au and Te, and rim is rich in Se and Pb.

Se and Te show broad-scale positive correlations with sulphur content (Figure 3), as do other trace elements including copper (Figure 3(C)). Lead does not show a well-developed correlation with sulphur, but instead exhibits a bimodal distribution of values (Figure 3 (D); most samples <40 ppm, seven others up to 600 ppm). Neither Se nor Te shows a positive correlation with total organic carbon content (Table 1).

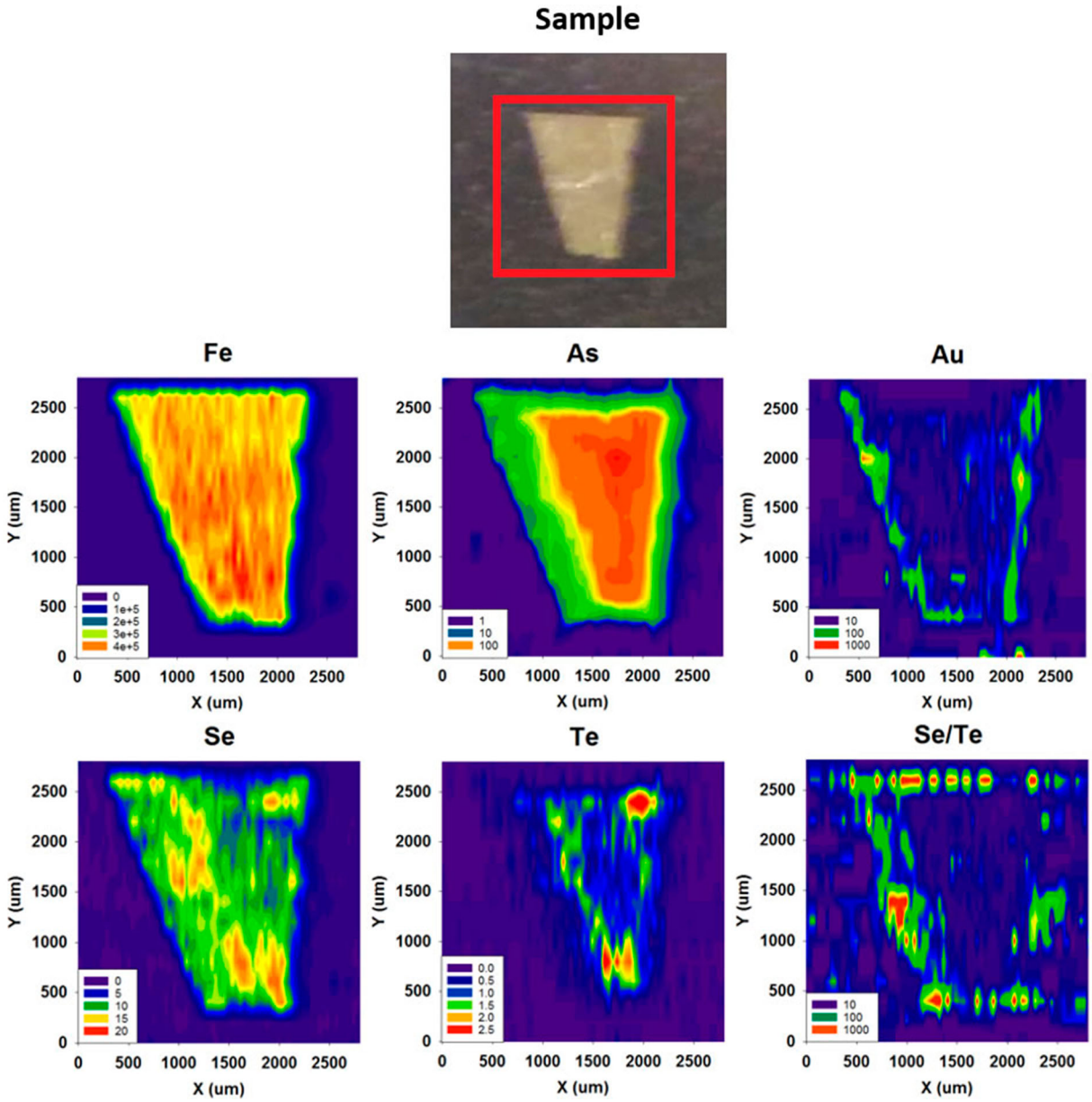

Figure 8. LA-ICP-MS element maps for pyrite crystal, Termon Pelite, Bellanamore, Ireland. Note Te through core, Au enriched in rim.

Mean whole rock analyses of the shales show that they contain trace element values exceeding (Ag, Cu, Co, Mo, Pb, Se, Te) or comparable with (Bi, Ni, Zn) those of global mean values for shales/pelites reported by Hu and Gao (2008) (Table 1). Whole rock rhenium/molybdenum (Re/Mo) ratios are mostly below 0.003 (Table 1).

SEM

The stoichiometry of sulphide crystals shows that at Strachur and Portsoy the dominant sulphide is pyrrhotite rather than pyrite (Figure 12). This was confirmed by observations in reflected light.

LA-ICP-MS

Mapping of trace elements in the pyrite crystals detected trace element contents higher than in the surrounding sedimentary (pelitic, psammitic) host, and showed simple zonation of content between early- and late-stage pyrite within some crystals. Examples of trace element maps and line profiles are shown in Figures 5–9. Typical patterns observed include:

(i) Arsenic contents higher in the core than in the rim (Figure 5).
(ii) Gold and Te at detectable level in the cores (Figures 6 and 7).
(iii) Selenium contents higher in the core than in the rim, or higher in the rim than in the core, or uniform across the pyrite (Figures 6 and 7).
(iv) Gold-rich rims (Figure 8 and 9).
(v) Lead-rich rims (Figures 5–7).

In the samples from two localities with pyrrhotite mineralisation (Strachur, Portsoy), the content of

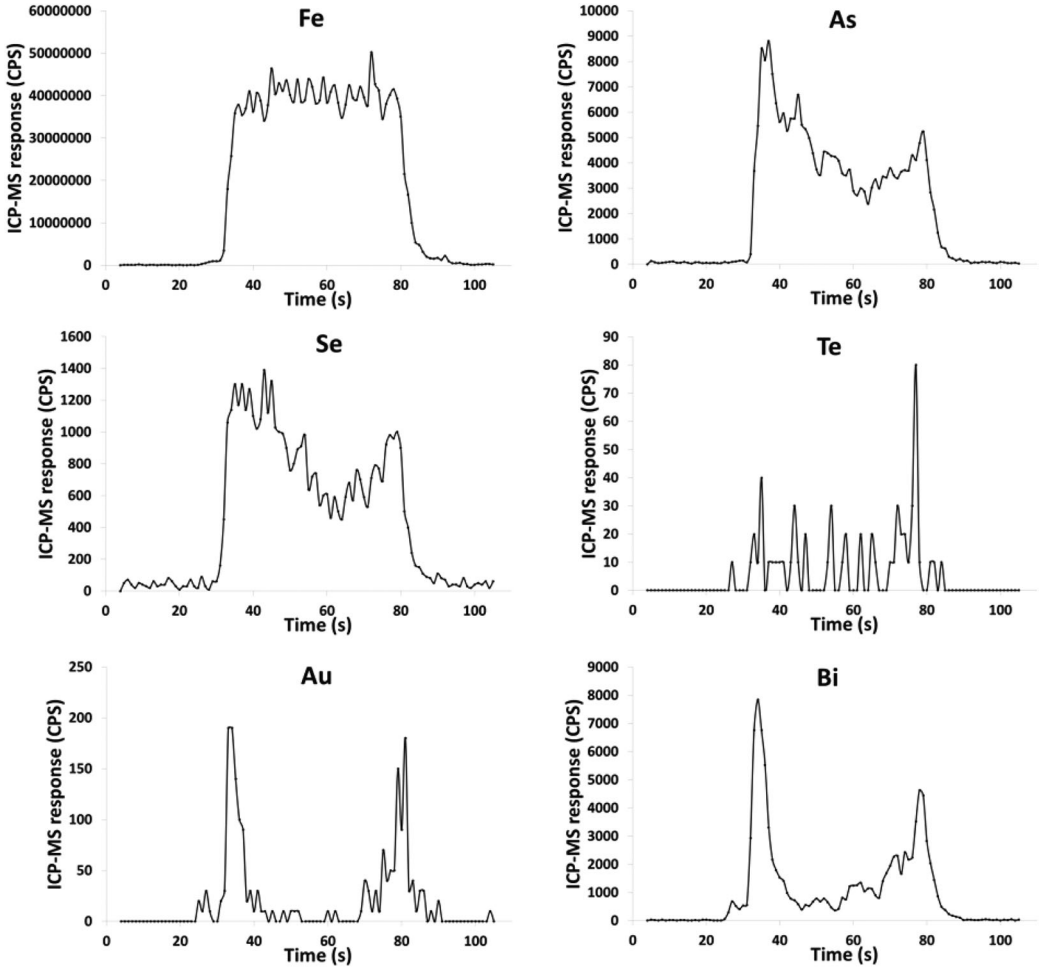

Figure 9. LA-ICP-MS profiles for elements along a linear track through a pyrite crystal, Termon Pelite, Bellanamore, Ireland. Note enrichments in most elements, including gold, in rims of crystal.

trace elements in the sulphide is relatively low compared to that in pyrite at other localities (Figure 10). The six pyrrhotite samples all have Se contents among the 10 lowest values of 26 samples (Figure 10), and no detectable Au. Four of the pyrrhotites also have very low Te contents (Figure 10).

Pyrite in other black shale samples analysed in the same laboratory does not show the gold signature

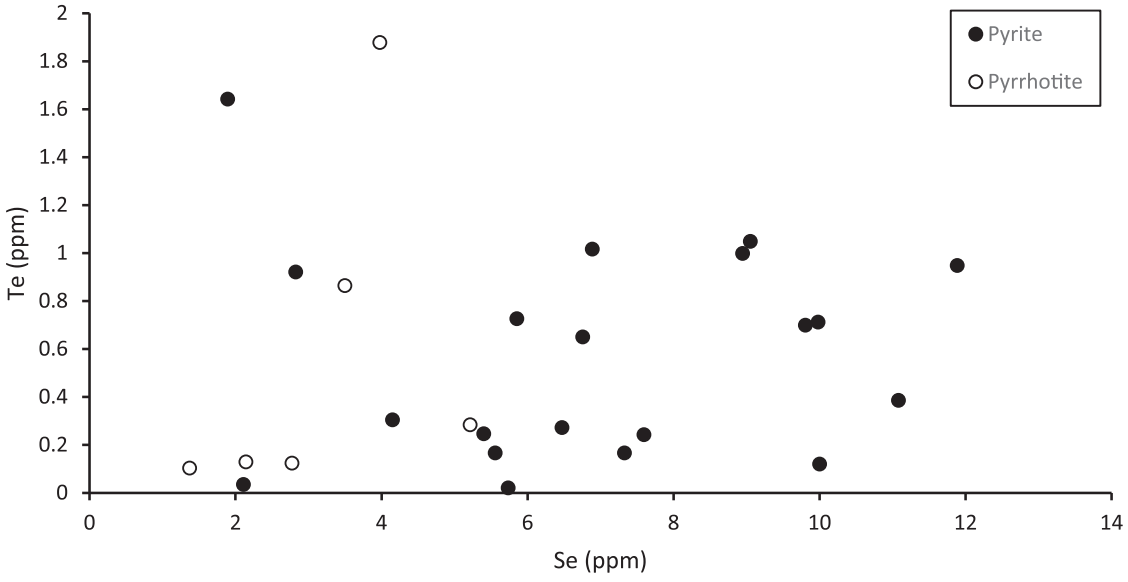

Figure 10. Cross-plots of Se and Te contents in sulphide crystals, determined by LA-ICP-MS. Samples of pyrrhotite have relatively low contents compared with the samples of pyrite.

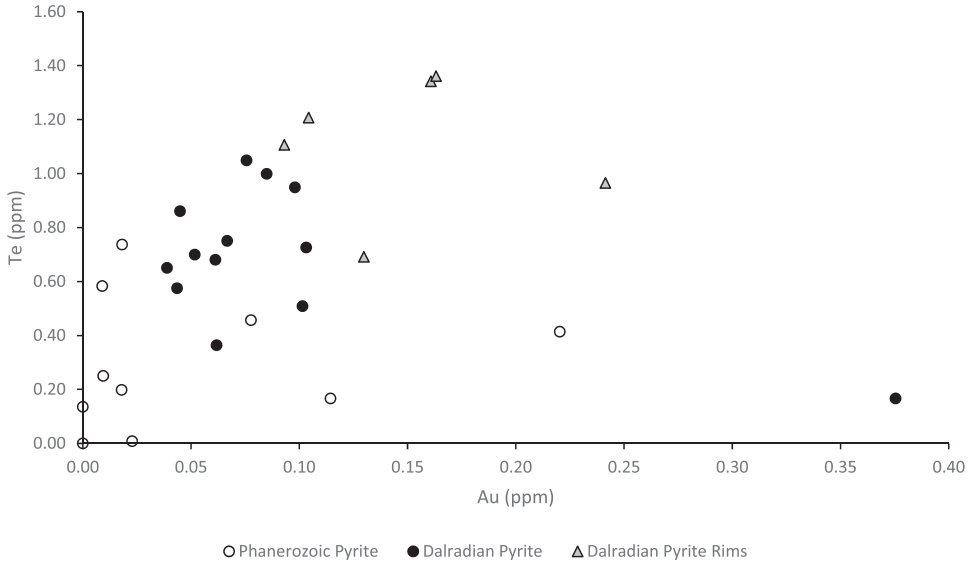

Figure 11. Cross-plot of Te and Au contents in pyrite in Dalradian black shales from Bellanamore, and in Phanerozoic (Ordovician and Carboniferous) black shales from Britain and Ireland, measured by LA-ICP-MS. Values in Dalradian pyrite are generally higher than in Phanerozoic pyrite. Enriched rims of Dalradian pyrite are shown separately.

detected in the Dalradian-hosted samples. Semi-quantitative measurements of Au in the Dalradian-hosted pyrite from Bellanamore indicate values mostly in the range 0.05–0.1 ppm, while less Au was detected in most pyrite in samples from the Phanerozoic (Carboniferous and Ordovician) of Britain and Ireland (Figure 11). The rims of the Bellanamore pyrite are further enriched in Au, mostly in the range 0.1–0.2 ppm (Figure 11).

S isotopes

Measurements of S isotopes showed wide variations in composition. The Easdale Slate-hosted pyrite at Easdale yields positive compositions of +11.3 and +11.8‰, consistent with published values in the range +12.4 to +14.1 ‰ ($n = 4$) (Hall et al. 1988), while the Craignish Phyllite-hosted pyrite yielded light (negative) compositions (−15.5 ‰, Loch Melfort, Scotland; −16.5, −17.1 and −18.1 ‰ in equivalent Termon Pelite, Bellanamore, Ireland).

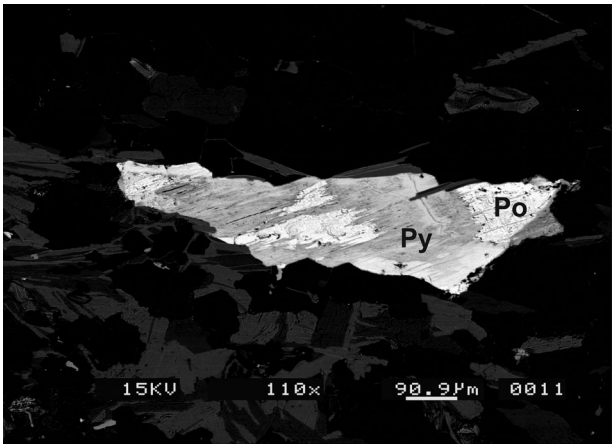

Figure 12. Backscattered electron micrograph of pyrite (Py) partially replaced by pyrrhotite (Po), in Dalradian carbonaceous shale, Strachur.

Discussion

Trace element residence in sulphides

The whole rock data show that trace element content is broadly correlated with sulphur contents, implying they are located in sulphide minerals, especially pyrite. LA-ICP-MS mapping further shows that trace elements, including Au, are concentrated in the pyrite. Line profiles from host into pyrite crystals show much higher trace element counts within the pyrite (Figure 5). The high sulphur levels in the Easdale Subgroup (Bata and Parnell 2014; Moles et al. 2014) have thus engendered a high concentration of metals, including Au, through pyrite formation.

Previous laser data for pyrite in Dalradian pelites (Pitcairn et al. 2015) showed lower Au contents in pyrite from rocks at higher metamorphic grade, implying mobility of Au due to regional metamorphism. This previous data set was not specifically for carbonaceous shales.

Pyrite formation

Previous studies in the Easdale Subgroup have shown that early diagenetic pyrite framboids are overgrown by later euhedral pyrite (Hall et al. 1988). More generally, images show an inner inclusion-rich pyrite followed by a euhedral inclusion-poor overgrowth (Hall et al. 1994). The inclusions in the earlier pyrite include chalcopyrite, sphalerite and galena. Sulphur isotope data suggest that the original pyrite was syn-diagenetic,

but may have been subsequently recrystallised (Hall et al. 1988, 1994). The whole rock Re/Mo values for the shales indicate deposition in an anoxic environment (Crusius et al. 1996). Despite some recrystallisation of the first phase, the two generations of pyrite are interpreted to represent a metal-rich anoxic depositional environment and metamorphic fluids. The early pyrite can be attributed to early burial (syn-diagenesis), as microbial sulphate reduction and pyrite precipitation are almost ubiquitous in organic-rich shales deposited in a marine environment. The euhedral pyrite is attributed to growth during metamorphism.

The mapping of element distribution by LA-ICP-MS in this study similarly suggests a distinction between early and late pyrite. Early pyrite in modern anoxic environments is typically enriched in trace elements (e.g. Scholz and Neumann 2007). In metamorphosed successions, pyrite typically exhibits euhedral overgrowths upon anhedral syn-diagenetic pyrite (Large et al. 2009). The pyrite in the Dalradian Supergroup exhibits overgrowths that are, accordingly, attributed to metamorphism. Regional metamorphism is dated at late Cambrian to Ordovician (Friedrich et al. 1999; Oliver et al. 2000; Bird et al. 2013), in advance of the gold mineralisation dated between Ordovician and Devonian (Treagus et al. 1999; Rice et al. 2016).

Trace element patterns in pyrite

The data show evolution of the trace element geochemistry between the early and late stages of pyrite growth. Arsenic occurs at higher levels in the early-stage pyrite, and some early pyrite contains Au and Te. Gold, Te and Pb occur at higher levels in some examples of later stage pyrite. Selenium occurs at relatively uniform levels, but can also exhibit enrichment in the rims, especially where the rims are also Pb-rich, suggesting that the Se may occur as micro-inclusions of Pb selenide. These patterns are comparable with those detected in other examples of multi-stage pyrite in carbonaceous sediments, which show that As levels tend to be highest in syn-diagenetic pyrite, Te and Se show distinct patterns, and Se is likely to be the most uniformly precipitated (Large et al. 2009; Gregory et al. 2015). Examples of Au-rich early pyrite and Au-rich rims are both recorded elsewhere (Large et al. 2009). Overall, the trace element contents of early pyrite are commonly higher than in late pyrite. This is consistent with data from other black shale successions (Gregory et al. 2015).

Pyrrhotite

The trace element content in the pyrrhotite is relatively low (Figure 10). Studies of other examples of pyrrhotite show that trace elements are released during the conversion of pyrite to pyrrhotite (Pitcairn et al. 2006, 2015; Thomas et al. 2011; Large et al. 2014). The data reported here are consistent with liberation of elements during pyrrhotite formation, during regional metamorphism. The two pyrrhotite-bearing localities are both in regions of amphibolite facies, whereas most pyrite was sampled from two regions of greenschist facies (Table 1). This suggests that pyrrhotite formation contributed to the availability of Au and other elements for mineralisation, independent of magmatic activity. In the two pyrrhotite samples which have relatively high Te contents (Figure 10), the Te may be present as telluride micro-inclusions which survived the conversion.

Gold and tellurium

The LA-ICP-MS maps and profiles show that both Au and Te occur in early pyrite. The occurrences of Au and Te in the early pyrite are anomalously rich, compared to measurements made on pyrite in shales of other ages in the same laboratory (Figure 11). The values for Au in the Dalradian pyrite are higher than values in a global database for sedimentary pyrite (Gregory et al. 2015), which indicate a mean value of 0.026 ppm Au. They are also higher than values for pyrite in a broader (stratigraphically and carbon content) data set for the Dalradian reported by Pitcairn et al. (2015), of which less than 3% exceeded 0.1 ppm Au. The Te levels in the data set from Bellanamore are also higher than in the Phanerozoic data set. Gold also occurs at relatively rich levels in the rims of late-stage pyrite (Figure 11), where it may be related to Te (Figure 11) or unrelated to Te (Figure 9), while Te also occurs in point source concentrations in the late-stage pyrite. The data as a whole show that both Au and Te were concentrated in the shale at an early stage, then mobilised and further concentrated at a later stage. This is consistent with a correlation between the two elements in a global database, although a Te/Au ratio of ~10 in the database shows that the Au resides in the telluride of another metal (Large et al. 2015). Tellurium whole rock content increases with Bi contents (Figure 4(B)), suggesting that Te occurs as sub-micron Bi tellurides.

Where trace elements including Au are concentrated in the overgrowths in the Dalradian pyrite (Figure 8), attribution of the overgrowths to metamorphism dates element mobility to the Cambro-Ordovician. This is not necessarily an episode of ore mineralisation. It does, however, demonstrate that there was an anomalous amount of Au in the Easdale Subgroup that was available for subsequent further concentration by hydrothermal activity. Thus, there was a source of metal from within the Dalradian succession, prior to the Cambro-Ordovician metamorphism and magmatic activity, and to the later Au mineralisation. Pyrite rich in trace elements is particularly susceptible to dissolution (Savage et al. 2000; Diehl et al. 2012). Thus, there is

potential for the release of the trace elements during metamorphism and hydrothermal activity, and unrelated to magmatic activity.

Lead

Enrichments of Pb occur especially in the outermost rim of pyrite samples (Figures 5–7). This explains the bimodal distribution of Pb values (Figure 3(D)), which are high where a late rim is present. This pattern of late Pb precipitation could relate to hydrothermal Pb vein mineralisation that occurs across the Dalradian outcrop, but especially in SW Scotland (Pattrick and Russell 1989). The Pb veins may be younger than the Au mineralisation, of Carboniferous age (Pattrick 1985). However, galena deposition also occurred during Au mineralisation (Jenkin et al. 2017), and at Cononish Pb concentration correlates to Au grade (Earls et al. 1992). Lead (±Se) enrichment in rims usually coincides with Au and Te enrichment at the resolution of measurement, and there is a broad correlation of Te with Pb except for the highest Pb values (Figure 4(C)). However, maps of Se/Te and Pb/Au ratios show an outer rim of elevated Se/Te and Pb/Au, indicating that Se and Pb mobility continued after Te and Au mobility (Figure 6). The enriched rims are consistent with the concentration of trace elements during metamorphism, and availability of all elements to ore mineralisation.

Sulphur isotope compositions

The positive and negative compositions determined for pyrite in the Easdale Slate and Craignish Phyllite respectively are consistent with previous data for these units (Willan and Coleman 1983; Hall et al. 1988, 1994; Parnell et al. 2013), which attribute pyrite formation to microbial sulphate reduction. The correlation with previous data and the marked variation of sulphur isotope composition with Dalradian stratigraphy together strongly indicate an origin through low-temperature sulphate reduction, rather than a late uniform imprint. The S isotope composition of pyrite is preserved, and only locally homogenised, during metamorphism (Hall et al. 1994; Chang et al. 2008), so that stratigraphic variations are retained. The attribution of the pyrite to microbial sulphate reduction means that biogenic activity was critical to the initial stage of metal sequestration, which eventually resulted in ore formation.

Models for mineralisation in the Dalradian Supergroup

Previous evaluations of Au-Te mineralisation in the Dalradian Supergroup have concluded that magmatic activity was at least partially responsible (Curtis et al. 1993; Parnell et al. 2000; Tanner 2012; Hill et al. 2014). Tellurium enrichment in the Curraghinalt deposit, Northern Ireland, suggests a possible granitic source (Rice et al. 2016). Comparisons of sulphur isotope compositions in pyrite from ore deposits and the Dalradian metasedimentary rocks suggest variable levels of mixing between magmatic sulphur and sedimentary sulphur (Pattrick et al. 1988; Hill et al. 2011, 2014; Graham et al. 2017). Pyrite-rich carbonaceous sediments in the Easdale Subgroup are particularly implicated as a source of sedimentary sulphur. The Easdale Subgroup has been similarly proposed as a source of metals to the ore mineralisation (Plant et al. 1997; Hill et al. 2014). The data reported in this study, showing metal enrichment in the original sediments, and subsequent mobilisation and further concentration, provide evidence to support this model involving a sedimentary source. The data do not require a magmatic source, but also do not exclude such a source. Other evidence for mobility of gold during metamorphism (Pitcairn et al. 2015) is consistent with the new data.

The consistent evidence of Pb enrichment in the outer parts of pyrite crystals are evidence of late-stage Pb mobilisation. Vein Pb mineralisation occurs across much of the Dalradian outcrop of SW Scotland and NW Ireland, and the data for the pyrite may be an expression of this episode. This relationship could be investigated further by comparison of pyrite trace element compositions in shales and cross-cutting mineral veins.

Conclusions

The geochemical data for the Dalradian carbonaceous shales show that they are a viable protolith for Dalradian-hosted gold-tellurium mineralisation. In particular:

(i) Trace element concentrations, including Au and Te, in early-stage pyrite show that ore metal concentration began in the organic-rich sediments of the depositional environment.
(ii) Further enrichment of Au and Te occurred in the rims of some pyrite samples, indicating mobility and concentration during metamorphism and related hydrothermal fluid flow.
(iii) In some samples, Au and Te enrichment in the rims is associated also with Pb enrichment, although subsequent Au/Te and Pb ore mineralisations are not necessarily coeval.
(iv) Absence of Au, and generally low levels of trace elements including Te, in pyrrhotite, implies their liberation during the conversion from pyrite to pyrrhotite.

This study reinforces previous evidence that microbial sulphate reduction is the starting point that leads ultimately to Au-Te ore formation in black shale sequences (Chang et al. 2008; Tomkins 2013), and

supports a more general model of Au concentration in pyritic, carbonaceous sediments (Pitcairn 2011; Gaboury 2013; Tomkins 2010, 2013). Early pyrite formation provides the feedstock that can then be progressively concentrated through diagenesis, metamorphism and hydrothermal activity. High sulphur content in the seawater, as evidenced by exhalative barite in the Dalradian Argyll Group (Moles et al. 2014), led to extensive pyrite precipitation and made the succession an especially fertile one for Au mineralisation.

Acknowledgements

Reviews by Iain Pitcairn and an anonymous reviewer helped to improve the manuscript.

Disclosure statement

No potential conflict of interest was reported by the authors.

Funding

This work was supported by the NERC under Grant number NE/L001764/1. AJB is funded by NERC support of the Isotope Community Support Facility at SUERC.

ORCID

J. Parnell http://orcid.org/0000-0002-5862-6933

References

Anderton R. 1985. Sedimentation and tectonics in the Scottish Dalradian. Scot J Geol. 21:407–436.

Bata T, Parnell J. 2014. A Neoproterozoic petroleum system in the Dalradian Supergroup, Scottish Caledonides. J Geol Soc Lond. 171:145–148.

Bird AF, Thirlwall MF, Strachan RA, Manning CJ. 2013. Lu-Hf and Sm-Nd dating of metamorphic garnet: evidence for multiple accretion events during the Caledonian Orogeny in Scotland. J Geol Soc Lond. 170:301–317.

Chang Z, Large RR, Maslennikov V. 2008. Sulfur isotopes in sediment-hosted orogenic gold deposits: evidence for an early timing and a seawater sulfur source. Geology. 36:971–974.

Craw D, Chamberlain CP. 1996. Meteoric incursion and oxygen fronts in the Dalradian metamorphic belt, southwest Scotland: a new hypothesis for regional gold mobility. Miner Deposita. 31:365–373.

Crusius J, Calvert S, Pedersen T, Sage D. 1996. Rhenium and molybdenum enrichments in sediments as indicators of oxic, suboxic and sulfidic conditions of deposition. Earth Planet Sc Lett. 145:65–78.

Curtis SF, Pattrick RAD, Jenkin GRT, Fallick AE, Boyce AJ, Treagus JE. 1993. Fluid inclusion and stable isotope study of fault-related mineralization in Tyndrum area, Scotland. Inst Min Metall Trans. 102:B39–B47.

Dempster TJ, Rogers G, Tanner PWG, Bluck BJ, Muir RJ, Redwood SD, Ireland TR, Paterson BA. 2002. Timing and deposition, orogenesis and glaciation within the Dalradian rocks of Scotland: constraints from U-Pb ages. J Geol Soc Lond. 159:83–94.

Diehl SF, Goldhaber MB, Koenig AE, Lowers HA, Ruppert LF. 2012. Distribution of arsenic, selenium, and other trace elements in the high pyrite Appalachian coals: evidence for multiple episodes of pyrite formation. Int J Coal Geol. 94:238–249.

Earls G, Parker RTG, Clifford JA, Meldrum AH. 1992. The geology of the Cononish gold-silver deposit, Grampian Highlands, Scotland. In: Bowden AA, editor. Irish minerals industry 1980-1990. Dublin: Irish Association for Economic Geology; p. 89–103.

Fettes, DJ. 1979. A metamorphic map of the British and Irish Caledonides. In: Harris AL, Holland CH, Leake BE, editors. The Caledonides of the British Isles reviewed, Vol. 8. London: Geological Society of London, Special Publication; p. 307–321.

Friedrich AM, Hodges KV, Bowring SA, Martin MW. 1999. Geochronological constraints on the magmatic, metamorphic and thermal evolution of the Connemara Caledonides, western Ireland. J Geol Soc Lond. 156:1217–1230.

Gaboury D. 2013. Does gold in orogenic deposits come from pyrite in deeply buried carbon-rich sediments? Insight from volatiles in fluid inclusions. Geology. 41:1207–1210.

Goldfarb RJ, Groves DI. 2015. Orogenic gold: common or evolving fluid and metal sources through time. Lithos. 233:2–26.

Graham SD, Holwell DA, McDonald I, Jenkin GRT, Hill NJ, Boyce AJ, Smith J, Sangster C. 2017. Magmatic Cu-Ni-PGE-Au sulphide mineralisation in alkaline igneous systems: an example from the Sron Garbh intrusion, Tyndrum, Scotland. Ore Geol Rev. 80:961–984.

Gregory DD, Large RR, Halpin JA, Baturina EL, Lyons TW, Wu S, Danyushevsky L, Sack PJ, Chappaz A, Maslennikov VV, Bull SW. 2015. Trace element content of sedimentary pyrite in black shales. Econ Geol. 110:1389–1410.

Hall AJ. 1993. Stratiform mineralization in the Dalradian of Scotland. In: Pattrick RAD, Polya DA, editors. Mineralization in the British Isles. London: Chapman & Hall; p. 38–101.

Hall AJ, Boyce AJ, Fallick AE. 1988. A sulphur isotope study of iron sulphides in the Late Precambrian Dalradian Easdale Slate Formation, Argyll, Scotland. Mineral Mag. 52:483–490.

Hall AJ, Boyce AJ, Fallick AE. 1994. A sulphur isotope study of iron sulphides in the late Precambrian Dalradian Ardrishaig Phyllite Formation, Knapdale, Argyll. Scot J Geol. 30:63–71.

Harte B. 1988. Lower Palaeozoic metamorphism in the Moine-Dalradian belt of the British Isles. In: Harris AL, Fettes DJ, editors. The Caledonide-Appalachian Orogen, Vol. 38. Geological Society, London, Special Publications; p. 123–134.

Hill NJ, Jenkin GRT, Boyce AJ, Sangster CJS, Catterall DJ, Holwell DA, Naden J, Rice CM. 2014. How the Neoproterozoic S-isotopic record illuminates the genesis of vein gold systems: an example from the Dalradian Supergroup in Scotland. In: Jenkin GRT, Lusty PAJ, McDonald I, Smith MP, Boyce AJ, Wilkinson JJ, editors. Ore deposits in an evolving earth, Vol. 393. Geological Society, London, Special Publication; p. 213–247.

Hill NJ, Jenkin GRT, Holwell DA, Matthews KE, Moore P, Catterall D, Boyce AJ, Mark DF, Gunn G, Naden J, et al. 2011. New gold occurrences in the Scottish Dalradian, UK – nature and constraints on genesis. In: Let's Talk Ore Deposits, 11th SGA Biennial Meeting, Antofagasta, Chile; p. 575–577.

Hu X, Gao S. 2008. Upper crustal abundances of trace elements: A revision and update. Chem Geol. 253:205–221.

Jenkin GRT, Spence-Jones C, Boyce AJ, Hill NJ, Sangster CJS. 2017. An early magmatic fluid pulse at Cononish orogenic gold deposit? Tellurium enrichment and implications for orogenic gold formation. Proceeding of the 14th SGA Biennial Meeting, Aug 20–23, 2017; Québec City, Canada; p. 1301–1304.

Large RR, Danyushevsky L, Hollit C, Maslennikov V, Meffre S, Gilbert S, Bull S, Scott R, Emsbo P, Thomas H, et al. 2009. Gold and trace element zonation in pyrite using a laser imaging technique: implications for the timing of gold in orogenic and Carlin-style sediment-hosted deposits. Econ Geol. 104:635–668.

Large RR, Gregory DD, Steadman JA, Tomkins AG, Lounejeva E, Danyushevsky LV, Halpin JA, Maslennikov V, Sack PJ, Mukherjee I, et al. 2015. Gold in the oceans through time. Earth Planet Sc Lett. 428:139–150.

Large RR, Hapin JA, Danyushevsky LV, Maslennikov VV, Bull SW, Long JA, Gregory DD, Lounejeva E, Lyons TW, Sack PJ, et al. 2014. Trace element content of sedimentary pyrite as a new proxy for deep-time ocean-atmosphere evolution. Earth Planet Sci Lett. 389:209–220.

Large RR, Maslennikov V, Robert F, Danyushevsky LV, Chang Z. 2007. Multistage sedimentary and metamorphic origin of pyrite and gold in the giant Sukhoi Log deposit, Lena gold province, Russia. Econ Geol 102:1232–1267.

Moles NR, Boyce AJ, Fallick AE. 2014. Abundant sulphate in the Neoproterozoic ocean: implications of constant δ34S barite in the Aberfeldy SEDEX deposits, Scottish Dalradian. In: Jenkin GRT, Lusty PAJ, McDonald I, Smith MP, Boyce AJ, Wilkinson JJ, editors. Ore deposits in an evolving earth, Vol. 393. Geological Society, London: Special Publication; p. 189–212.

Oliver GJH, Chen F, Buchwald R, Heger E. 2000. Fast tectonothermal metamorphism and exhumation in the type area of the Barrovian and Buchan zones. Geology. 28:459–462.

Parnell J, Boyce AJ, Hurst A, Davidheiser-Kroll B, Ponicka J. 2013. Long term geological record of a global deep subsurface habitat in sand injection complexes. Sci Rep. doi:10.1038/srep01828.

Parnell J, Earls G, Wilkinson JJ, Hutton DHW, Boyce AJ, Fallick AE, Ellam RM, Gleeson SA, Moles NR, Carey PF, et al. 2000. Regional fluid flow and gold mineralization in the Dalradian of the Sperrin Mountains, Northern Ireland. Econ Geol. 95:1389–1416.

Pattrick RAD. 1985. Pb-Zn and minor U mineralization at Tyndrum, Perthshire. Mineral Mag. 49:671–681.

Pattrick RAD, Boyce A, Macintyre RM. 1988. Au-Ag vein mineralization at Tyndrum, Scotland. Miner Petrol. 38:61–76.

Pattrick RAD, Russell MJ. 1989. Sulphur isotopic investigation of Lower Carboniferous vein deposits of the British Isles. Miner Deposita. 24:148–153.

Pitcairn IK. 2011. Background concentrations of gold in different rock types. Appl Earth Sci. 120:31–38.

Pitcairn IK, Skelton ADL, Wohlgemuth-Ueberwasser CC. 2015. Mobility of gold during metamorphism of the Dalradian in Scotland. Lithos. 233:69–88.

Pitcairn IK, Teagle DAH, Craw D, Olivo GR, Kerrich R, Brewer TS. 2006. Sources of metals in orogenic gold deposits: insights from the Otago and Alpine Schists, New Zealand. Econ Geol. 101:1525–1546.

Plant JA, Stone P, Flight DMA, Green PM, Simpson PR. 1997. Geochemistry of the British Caledonides: the setting for metallogeny. Trans Inst Min Metall. 106:B67–B78.

Prave AR, Fallick AE, Thomas CW, Graham CM. 2009. A composite C-isotope profile for the Neoproterozoic Dalradian Supergroup of Scotland. J Geol Soc Lond. 166:845–857.

Rice CM, Mark DF, Selby D, Neilson JE, Davidheiser-Kroll B. 2016. Age and geologic setting of quartz vein-hosted gold mineralization at Curraghinalt, Northern Ireland: implications for genesis and classification. Econ Geol. 111:127–150.

Robinson BW, Kusakabe M. 1975. Quantitative preparation of sulfur dioxide for $^{34}S/^{32}S$ analyses from sulphides by combustion with cuprous oxide. Anal Chem. 47:1179–1181.

Savage KS, Tingle TN, O'Day PA, Waychunas GA, Bird DK. 2000. Arsenic speciation in pyrite and secondary weathering phases, Mother Lode Gold District, Tuolumne County, California. Appl Geochem. 15:1219–1244.

Scholz F, Neumann T. 2007. Trace element diagenesis in pyrite-rich sediments of the Achterwasser lagoon, SW Baltic Sea. Mar Chem. 107:516–532.

Stephenson D, Mendum JR, Fettes DJ, Leslie AG. 2013. The Dalradian rocks of Scotland: an introduction. P Geologist Assoc. 124:3–82.

Stüeken EE, Buick R, Bekker A, Catling D, Foriel J, Guy BM, Kah LC, Machel HG, Montañez IP, Poulton SW. 2015. The evolution of the global selenium cycle: Secular trends in Se isotopes and abundances. Geochim Cosmochim Acta. 162:109–125.

Tanner PWG. 2012. The giant quartz-breccia veins of the Tyndrum-Dalmally area, Grampian Highlands, Scotland: their geometry, origin and relationship to the Cononish gold-silver deposit. Earth Environ Sci Trans Royal Soc Edinburgh. 103:51–76.

Thomas HV, Large RR, Bull SW, Maslennikov V, Berry RF, Fraser R, Froud S, Moye R. 2011. Pyrite and pyrrhotite textures and composition in sediments, laminated quartz veins, and reefs at Bendigo gold mine, Australia: insights for ore genesis. Econ Geol. 106:1–31.

Tomkins AG. 2010. Windows of metamorphic sulfur liberation in the crust: implications for gold deposit genesis. Geochim Cosmochim Acta. 74:3246–3259.

Tomkins AG. 2013. A biogeochemical influence on the secular distribution of orogenic gold. Econ Geol. 108:193–197.

Treagus JE, Pattrick RAD, Curtis SF. 1999. Movement and mineralization in the Tyndrum Fault Zone, Scotland and its regional significance. J Geol Soc Lond. 156:591–604.

Turekian KK, Wedepohl KH. 1961. Distribution of the elements in some major units of the earth's crust. Geol Soc Amer Bull. 72:175–192.

Wagner T, Klemd R, Wenzel T, Mattsson B. 2007. Gold upgrading in metamorphosed massive sulphide ore deposits: direct evidence from laser-ablation-inductively couple plasma-mass spectrometry analysis of invisible gold. Geology. 35:775–778.

Willan RCR, Coleman ML. 1983. Sulfur isotope study of the Aberfeldy barite, zinc, lead deposit and minor sulfide mineralization in the Dalradian metamorphic terrain, Scotland. Econ Geol. 78:1619–1656.

Wilson SA, Ridley WI, Koenig AE. 2002. Development of sulfide calibration standards for the laser ablation inductively-coupled plasma mass spectrometry technique. J Anal Atom Spectrom. 17:406–409.

Wyman DA, Cassidy KF, Hollings P. 2016. Orogenic gold and the mineral systems approach: resolving fact, fiction and fantasy. Ore Geol Rev. 78:322–335.